# DEVELOPMENT OF THE NASA MINI/MEMS TRI-AXIS SENSOR SYSTEM

*Kenneth G. Toro[1], and Jonathon D. Ponder[2]*
[1]NASA Langley Research Center, USA and
[2]NASA Glenn Research Center, USA

## ABSTRACT

This manuscript details the development of a reduced volume attitude sensor developed at NASA. This new sensor uses Micro Electro-Mechanical System (MEMS) based accelerometers to reduce the volume when compared to current sensors used in wind-tunnel models. Our team has designed, fabricated, and evaluated the Mini/MEMs Tri-Axis Sensor System (MTASS). The current MTASS design accommodates three high-precision accelerometers into the volume of a single-axis accelerometer that is currently used. This arrangement allows for the estimation of model pitch and roll angles. Static testing of the MTASS demonstrated angle accuracies within ±0.01° for both pitch and roll.

## KEYWORDS

Attitude Measurement, Aerodynamic Ground Testing, Calibration

## INTRODUCTION

Angle of attack, or attitude, is one of the critical measurements monitored and recorded during aerodynamic ground testing. Real-time attitude measurement of a test article is required for safety-of-flight systems used at tunnels to ensure real-time control of model attitude and position during experiments. Aerodynamics researchers demand high precision and accurate model attitude since it is directly related to aerodynamic performance. It is routinely accepted that an angle of attack accuracy of $\pm 0.01°$ is required to resolve a 0.0001 change in drag coefficient [1].

To provide the necessary accuracy, aerodynamic ground test facilities have mostly relied upon single-axis quartz accelerometers [2]. One commonly used sensor is the Honeywell QA-2000, which has a diameter and height of approximately 1-inch. Due to the volume of these quartz accelerometers, some small models cannot accommodate this class of sensor and typically forgoes any onboard attitude sensors. For these situations, an off-board measurement which consists of support system angle measurements and sting bending estimates based on force-measurements is used to determine model attitude.

Several smaller sensors have been tested at NASA Langley using MEMS based accelerometers [3, 4, 5]. Of these developed MEMS packages, none have been transitioned to production.

## SENSOR DEVELOPMENT

A survey of commercial-off-the-shelf (COTS) MEMS accelerometers identified a potential sensor to satisfy the requirements of wind-tunnel attitude measurements. A high-precision single-axis accelerometer was selected for further evaluation.

In accordance with recommendations from the accelerometer's datasheet, support circuits were designed. Internally, the accelerometer utilizes a capacitance-to-voltage converter based on a switched-capacitor architecture operating at 200kHz to provide a voltage readout from the varying capacitance due to movement of the accelerometer's proof-mass. The datasheet also specifies minimum input impedance requirements for the circuits connected to the acceleration high- and low-side outputs at 1 MΩ. It also specifies the maximum capacitive load of the acceleration and temperature outputs at 100pF and 10pF, respectively.

Through the capacitance-to-voltage converter, high-frequency noise on the accelerometer's supply voltage can alias into the device bandwidth. A compact, low-noise voltage reference was selected to power the accelerometer and conditioning circuits on the printed circuit board (PCB). In addition, the accelerometer output is ratiometrically dependent on the supply voltage, so stability was also considered when selecting the reference and evaluated on the single-axis PCB. While the reference is very stable over the entire operating temperature of the PCB, to increase accuracy and precision of the system, a buffered output of the reference voltage is provided to allow for ratiometric corrections to be applied by the acquiring system.

Since the 200kHz switching noise is still present on the output signal, a low-pass filter is required to remove it. The accelerometer signals are passed through a 2-pole Butterworth filter in a multiple feedback topology. Temperature signals use a 1-pole RC filter with an op-amp buffer. Each filter is built with high-precision op-amps and, in the case of the 2-pole, a matched resistor network to increase the precision of the system. The accelerometer datasheet provides guidelines for connected circuits. The connected circuit should have a minimum input impedance of 1 MΩ and utilize an op-amp with ultra-low offset, drift, and bias current. A zero-drift op-amp with 5pA bias current was selected. As is common with ultra-low bias current op-amps, the closed-loop output impedance of the selected op-amp increases rather sharply with frequency. Had a Sallen-Key topology, the manufacture's recommended circuit, been chosen for the 2-pole low-pass filter, this increasing closed-loop output impedance would have degraded the roll-off of the filter and caused it instead to begin increasing at higher frequencies. To counteract this effect, a follow-on RC low-pass filter would have been required and then a follow-on buffer to isolate the RC circuit from any connected system. A primary goal for the sensor was for it to be as small as possible, so to avoid the additional components required by the Sallen-Key topology, a Multiple Feedback (MFB) topology was selected instead. An advantage of the Sallen-Key topology over the MFB for unity gain is that resistor variance has no effect on gain. To mitigate this with the MFB topology, a quad matched resistor network with a value of 1 MΩ was used for the

high- and low-side low-pass filter gain setting resistors. The value of these resistors ensures that the input impedance of the low-pass filter circuit remains at or above 1 MΩ over the entire passband. A Sallen-Key topology, with similar value input resistors, would fall below the required 1 MΩ input impedance within the passband. As the MFB topology is inverting, a mid-span reference is required about which to invert the signal, this is provided by the selected voltage reference that powers the accelerometer and support circuits.

A single-axis board was designed to test the accelerometer with the custom support circuits. The PCB layout of the support circuits utilized the same dense component placement and trace routing that would be utilized on the follow-up rigid-flex tri-axis PCB. Evaluation of the single-axis board showed no compatibility issues between the accelerometer and support circuits. The single-axis PCBs were evaluated using a sine-plate and spin index. Evaluations were compared directly to a legacy, Q-flex based, accelerometer package to account for any test setup inaccuracies. Performance of the single-axis evaluation boards were found to be equivalent to the reference accelerometer.

In addition, single-axis PCBs with no accelerometer were utilized to evaluate the performance of the voltage reference and filter/buffer circuits over a -40˚F to 250˚F temperature range, as shown in Figure 1. The voltage reference was found to be stable to within +/- .01% over the range. The filter/buffer combined gain and offset was found to be within 15ppm over the entire range and better than 5ppm from -40˚F to 225˚F.

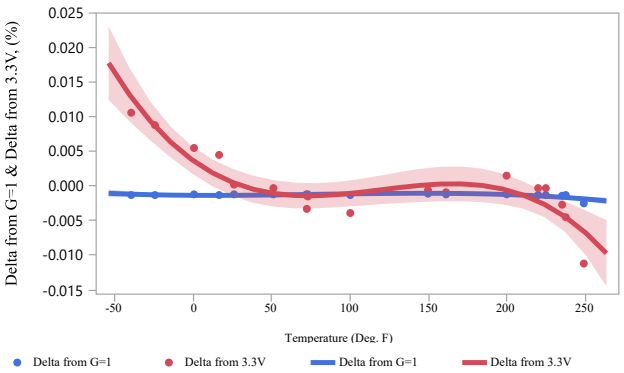



*Figure 1: Filter/buffer and 3.3V reference stability over operating temperature range.*

Following the performance evaluation of the single-axis PCBs, it was decided to proceed with the rigid-flex PCB design. The rigid-flex PCB is comprised of four 8-layer rigid panels connected by three 2-layer flexible polyimide sections. One rigid panel supports the input power conditioning, reference voltage generation and its buffered monitor output, and provides wiring interface pads on the opposite side. The remaining three rigid panels each hold an accelerometer and the required filter/buffer circuits on the opposite side. To facilitate the optimal placement of components and traces in the filter/buffer circuits, a sequential lamination process was used in PCB fabrication, which allows for vias that are both buried and blind. Those vias are connected to the outer layers via laser-drilled micro-vias.

The rigid-flex PCBs allowed for the three accelerometers to be positioned orthogonally. To complete the package, the board was bonded to a metallic frame using high-resistance epoxy resin. The tri-axis board and completed sensors are shown in Figure 2.

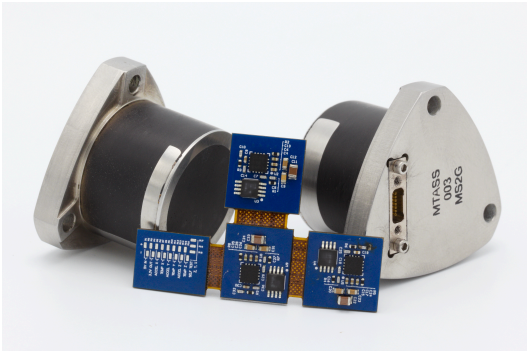



*Figure 2: MTASS tri-axis board in foreground with two fully fabricated systems in the background.*

## CALIBRATION METHOD AND MODELING

### Calibration Apparatus

The completed sensor was evaluated and calibrated on a custom two-axis index table manufactured by A.G. Davis, shown in Figure 3. This system comprises of two, high-precision, machinist index tables orientated such to allow setting combined pitch and roll angles. The system has the capability to position 360° combined angles in 1° increments within 2-arcsecond repeatability. Additionally, the system is assembled on an isolated concrete pier to provide a low noise and consistent platform.

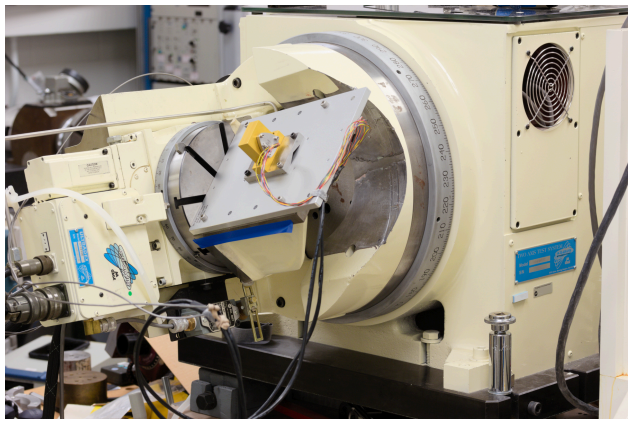


*Figure 3: View of the MTASS sensor on the two-axis index head during calibration.*

### Calibration Modeling and Data Reduction

It has been shown that tri-axis accelerometers with low nonlinearities can be modeled with a linear model [6, 7]

$$\boldsymbol{v} = \boldsymbol{\beta_0} + \boldsymbol{g}\boldsymbol{\beta_1} + \boldsymbol{\epsilon} \quad (1)$$

where $\boldsymbol{v}$ is a vector of measured accelerometer voltages, $\boldsymbol{\beta_0}$ is a vector of DC bias voltages, $\boldsymbol{g}$ is the gravity vector, $\boldsymbol{\beta_1}$ is a 3x3 calibration matrix, and $\boldsymbol{\epsilon}$ is a vector of errors. For a perfect sensor with pure orthogonality orientated accelerometers, the calibration matrix, $\boldsymbol{\beta_1}$, would be only a diagonal of the individual channel sensitivities. However,

most sensors will have cross-axis sensitives due to sensor alignment or inherent design properties. This would result in off-diagonal terms an order of magnitude smaller than the diagonal terms.

After solving Equation 1 for $\boldsymbol{g}$, the angles between the sensor coordinate system and earth can be found by

$$\alpha = \sin^{-1}(g_x),\ \phi = \tan^{-1}\left(\frac{g_y}{g_z}\right) \qquad (2)$$

where $\alpha$ and $\phi$ are the estimated pitch and roll angles. As the sensor approaches 90° pitch, roll angle cannot be defined and therefore a yaw angle should be estimated. In this manuscript low pitch angles will be examined to match to aerodynamics use case, which in many cases does not exceed $\pm 20°$.

**Experimental Design**

The minimal experimental design to provide enough degrees of freedom to fit Equation 1 is setting each axis, individually, to $\pm 1$g [6]. These types of points are considered axial, or star, points and when plotted lie directly on the axes. This bare minimum design does not allow for higher-order models or for lack of fit testing since no center point exists. A true center point, where all axes are set to zero, is not possible since gravity is always present. Using the two-axis index table, the applied gravity vector must lie on a sphere with radius one. Due to this constraint, all set points must have a root sum square of one. This constraint allows for the use of a spherical central composite design (SCCD) to allow for additional degrees of freedom for lack of fit or to support higher-order terms. The SCCD comprises the axial points with the addition of factorial points, where all three components are set to $\pm \frac{1}{\sqrt{3}}$g in combinations.

Additional points were added about two rotated planes, where the roll angle is 45° or 135°, to allow for further inspection of any non-linear sensor behavior. These additional points give a total of 11 set levels for each axis to observe detailed sensor behavior and repeatability. For a production calibration, these additional points would be unnecessary, since the SCCD would be sufficient for modeling purposes. The final experimental design used for sensor evaluation is shown in Figure 4. The experimental design was randomized to reduce the impact of systematic effects such as temperature or other temporal effects.

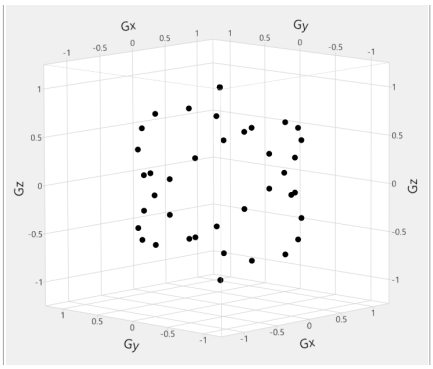



*Figure 4: MTASS experimental design in gravity component terms.*

## EXPERIMENTAL RESULTS

All experimental data in this manuscript were acquired on the calibration apparatus discussed in the previous section. Data were collected using a National Instruments PXI chassis with accelerometer voltage outputs on individual digital multi-meters (PXI-4071). Each data point comprises eight samples with the means electronically recorded for each calibration point. Each sensor was warmed up for several hours prior to stabilize the accelerometer outputs and voltage reference.

Two MTASS sensors, $\pm 2$g and $\pm 5$g variants, were tested on the two-axis index table using the described experimental design. Calibrations were repeated sequentially 10 times for both variants to investigate repeatability and short-term drift. In the results presented, the initial run is used to fit the calibration model as defined by Equation 1, and subsequent runs are purely validation. Results are presented as set angle position subtracted by back computed angles calculated by Equation 2.

Residual errors for pitch and roll estimates are shown in Figure 5 and Figure 6 for a pitch range of $\pm 55°$ and $\pm 180°$ roll for both the $\pm 2$g and $\pm 5$g variants. The results show an unintuitive difference between the different g ranges, where the $\pm 2$g sensor has higher residuals. This can be explained by exercising a lower full-scale range of the 5g sensor, and thus staying in a more linear portion of the sensor. If the 5g sensor was subjected to 2.5g a similar nonlinear behavior seen by the 2g sensor data could be observed. This behavior cannot be further explored due to the limits of our evaluation equipment.

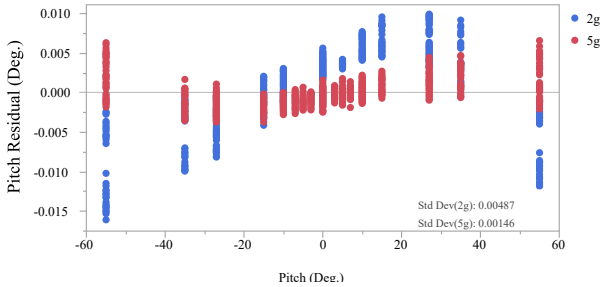



*Figure 5: Pitch residuals of the 2g and 5g MTASS sensor after calibration.*

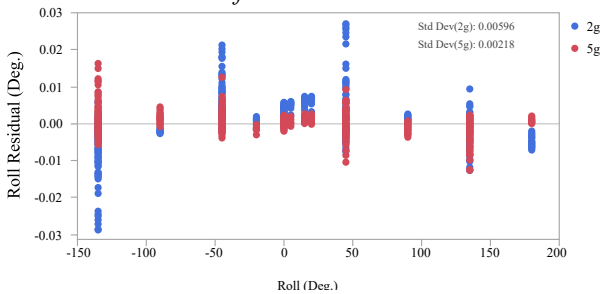



*Figure 6: Roll residuals of the 2g and 5g MTASS sensor after calibration.*

**Aerodynamic Ground Test Demonstration**

The NASA Ames Check Standard Model was designed to mount four Q-Flex sensors, two pitch and two roll sensors [8]. This model allowed for the opportunity to perform early demonstration testing of the MTASS sensor by occupying the secondary roll sensor location of this model. The $\pm 5$g variant was selected due to the lower nonlinearity and higher g range. Figure 7 shows the $\pm 5$g MTASS and a Q-Flex installed in the Check Standard Model balance block during model build up.

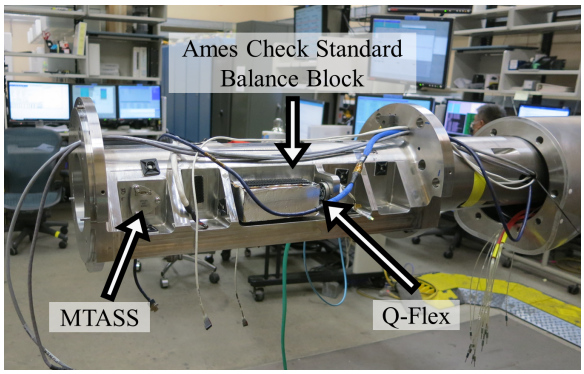



*Figure 7: View MTASS installed in the NASA Ames check standard model during instrumentation build up.*

The model pitch angle is measured using one of two Q-Flex sensors installed in the balance block. This primary sensor is used to calculate residuals for both the secondary Q-Flex and MTASS sensors as shown in Figure 8. This figure divides the residuals into five groups of dynamic pressure. Dynamic pressure is related to the wind-tunnel velocity and Mach number, where a higher dynamic pressure equates to higher aerodynamic forces on the model. It is seen that the MTASS sensor has larger residuals than the Q-Flex sensor, and a large increase at the highest dynamic pressures. Two main factors that may have contributed to the larger residuals are temperature and model dynamics. During the demonstration the sensor experienced temperatures between 70°F and 90°F.

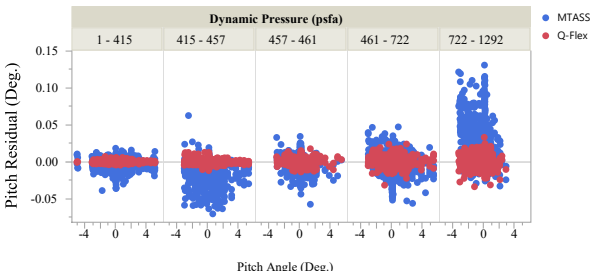



*Figure 8: Pitch residuals of the MTASS and secondary Q-Flex sensors during wind-tunnel testing of the Ames check standard model.*

During the wind-tunnel test campaign, loss of sensor signal occurred twice. Post-test it was found that the cable used for this demonstration had been improperly fabricated and resulted in loss of signal. Additionally, this issue may have impacted data quality. However, the overall results are promising given areas of improvement, such as temperature modeling.

## CONCLUSIONS

Laboratory evaluation of the complete sensor demonstrated accuracies below the ±0.01° threshold that is desired for aerodynamic ground testing. During this evaluation, the ±5g variant performance was better than the ±2g, due to observed lower nonlinearity. During wind-tunnel testing, the sensor had larger residuals than a Q-Flex sensor, although data quality may have been impacted due to a cabling issue discovered post-test. Despite the cable issue, the results are favorable to continue sensor development and additional characterizations. Further characterizations of the sensor are currently in planning, such as temperature corrections and dynamic testing.

## ACKNOWLEDGEMENTS

The authors would like to acknowledge Wentworth (Trevor) John, Timothy Dunlap, and Peter A. Parker. Trevor John greatly assisted with fabrication during the development of the sensor. Timothy Dunlap was instrumental to success of the assembly of the tri-axis system. Peter A. Parker provided insights and critical input to the project. This project was funded by NASA's Aerosciences Test and Evaluation Capability Portfolio Office, Test Technologies. We appreciate NASA Ames Unitary Plan Tunnel and Check Standard Model test team for the demonstration opportunity and their support.

## REFERENCES

[1] F. Steinle, E. Stanewsky, "Wind Tunnel Flow Quality and Data Accuracy Requirements", AGARD, 1982.

[2] T. Finley, P. Tcheng, "Model attitude measurements at NASA Langley Research Center", in *30th Aerospace Sciences Meeting and Exhibit*, Reno, January 6-9, 1992.

[3] R. Lawrence, S. Kahng, E. Adcock, H. Soto, W. Culliton, T. Jordan, C. Hernandez, S. Gorton, "MEMS sensor system development at NASA Langley Research Center for wind tunnel applications", in *40th AIAA Aerospace Sciences Meeting & Exhibit*, January, 2002.

[4] S. Yu and B. Newman, "Development of a High Accuracy MEMS Angular Measurement System for Hypersonic Wind Tunnel Facilities," in *44th IAA/ASME/ASCE/AHS/ASC Structures, Structural Dynamics, and Materials Conference*, April, 2003.

[5] B. Crawford, M. Rhode, "Miniature On-Board Angle of Attack Measurement System for Hypersonic Facilities", in *25th AIAA Aerodynamic Measurement Technology and Ground Testing Conference*, June, 2006.

[6] P. Parker, T. Finley, "Advancements in Aircraft Model Force and Attitude Instrumentation by Integrating Statistical Methods", in *AIAA Journal of Aircraft*, March, 2007.

[7] M. Gaitan, I.M.L. Bautista, J. Geist. "Reduction of calibration uncertainty due to mounting of three-axis accelerometers using the intrinsic properties model" in *Metrologia*, April, 2021.

[8] M. Amaya, R. Flach, T. Garbeff, "A Preliminary Investigation of the Check Standard Model in the NASA Ames Unitary Plan Wind Tunnel", in *AIAA Aviation 2019 Forum*, June, 2019.

## CONTACT

*K.G. Toro, tel: +1-757-864-3359;
kenneth.g.toro@nasa.gov
*J.D. Ponder, tel: +1-216-433-2816;
jonathon.d.ponder@nasa.gov

Trade names and trademarks are used in this report for identification only. Their usage does not constitute an official endorsement, either expressed or implied, by the National Aeronautics and Space Administration.